Lecture notes on topological insulators

Ming-Che Chang

Department of Physics, National Taiwan Normal University, Taipei, Taiwan

(Dated: January 7, 2021)

Contents

I. 3D TOPOLOGICAL INSULATOR

The analysis of the 2D TI can be generalized to 3D. One can naively stack the 2D materials to form a 3D structure (see Fig. 1). In early days, this has been attempted to build a 3D quantum Hall system, but failed. An essential reason is that there is no Chen number in odd dimension. The situation is different for the case of TI, where one can actually build a *weak* TI this way.

To simplify the discussion, consider a cubical BZ (see Fig. 2). If the insulator has TRS, then $\mathbf{k}$-state and $-\mathbf{k}$-state are TR conjugate. In particular, the points on the xy plane map to themselves under time reversal. According to the Moore-Balents argument, this plane should have a corresponding Z_2 index. Using Fu and Kane's formula, it is given by

$$(-1)^{\nu} = \delta_1\delta_2\delta_3\delta_4 \equiv z_0, \tag{1.1}$$

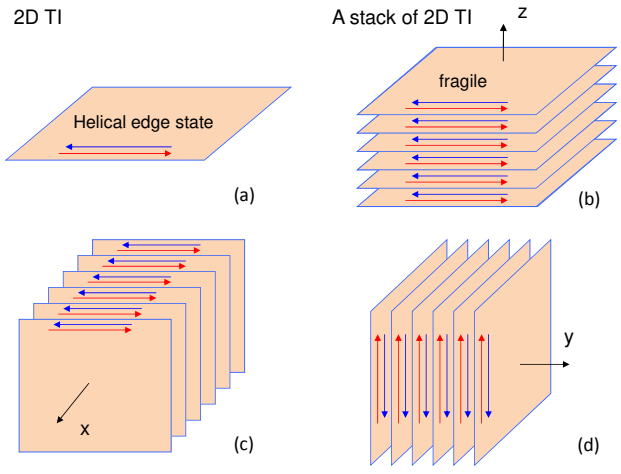

FIG. 1 (a) A 2D TI and its helical edge state. (b) Stacking 2D TIs to construct a 3D TI. The surface state is not as robust as the edge state of a 2D TI. (c) and (d): Stacking the 2D TIs along the other two directions. The helical edge states reside on different sides of the 3D cubes.

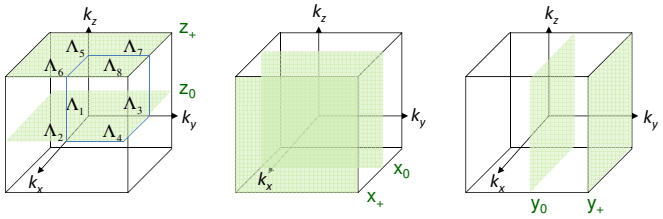

FIG. 2 The colored 2D planes in the 3D BZ are time reversal invariant. That is, under a TR transformation, they are mapped to themselves. There are all six of them. Each plane can be assigned a Z_2 topological number.

where $\delta_i = \prod_{n\in \text{ filled}} \zeta_n(\Lambda_i)$ (see Fig. 2).

By symmetry, the k_y-k_z plane and the k_z-k_x plane also have their own Z_2 indices, x_0 and y_0. In addition, the planes at front, right, and top side of the cube also map to themselves under time reversal. So there are three more Z_2 indices, x_+, y_+, and z_+. Overall there are 6 Z_2 numbers.

However, these numbers are not independent of each other,

$$x_0x_+ = y_0y_+ = z_0z_+ = \prod_{i=1}^{8}\delta_i. \tag{1.2}$$

Because of these two relations, there are only 4 independent Z_2 integers. One can choose, for example,

$$(z_0z_+, x_+, y_+, z_+) \quad \text{or} \quad (\nu_0;\nu_1,\nu_2,\nu_3), \tag{1.3}$$

where

$$(-1)^{\nu_0} = \prod_{i=1}^{8}\delta_i, \tag{1.4}$$
$$(-1)^{\nu_1} = \delta_2\delta_4\delta_6\delta_8, \tag{1.5}$$
$$(-1)^{\nu_2} = \delta_3\delta_4\delta_7\delta_8 \tag{1.6}$$
$$(-1)^{\nu_3} = \delta_5\delta_6\delta_7\delta_8. \tag{1.7}$$

Among these 4 indices, ν_0 is called **strong TI index**; ν_1,ν_2,ν_3 are called **weak TI indices**. The strong index is intrinsic to the 3D TI, while the other 3 are, roughly speaking, related to the stacking of 2D TIs along the x, y, and z directions (see Fig. 1). These indices are discovered by Moore and Balents, 2007, Fu *et al.*, 2007, and Roy, 2009 at about the same time.

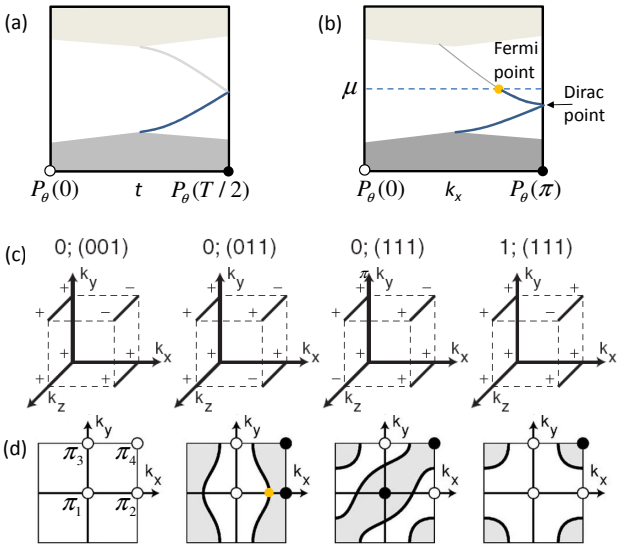

FIG. 3 (a) Energy levels of a 1D spin pump with an open edge, plotted as a function of time. The TR polarization P_θ at $t = 0, T/2$ are indicated by white dot (if $P_\theta = 0$) and black dot (if $P_\theta = 1$). (b) The energy dispersion of a 2D insulator on x-z plane, which has an open edge along z. The TR polarization at $k_x = 0, \pi$ are indicated by white dot (if $P_\theta = 0$) and black dot (if $P_\theta = 1$). (c) Four examples of the parity distributions at the TRIM (in the first octant of the BZ) of 3D TIs. (d) The Fermi seas in surface BZs of the four cases in (c). White and black dots at the corners show the values of P_θ being 0 or 1 (mod 2) along k_z (see text). The grey areas are filled, and the white areas are empty. (Figs (c), (d) from Fu and Kane, 2007)

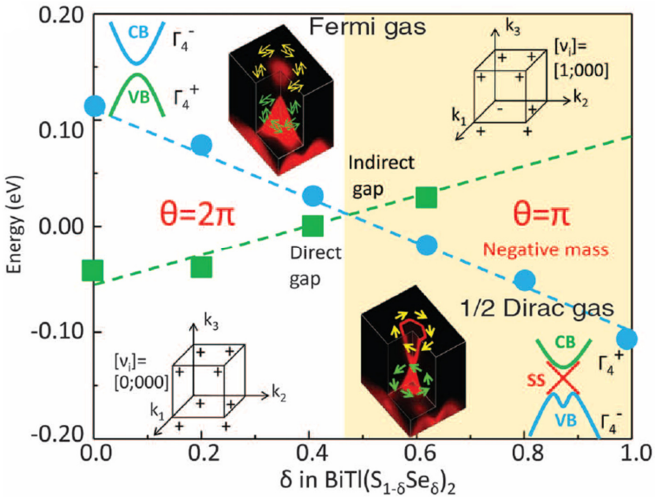

FIG. 4 Phase transition of topological insulator and accompanied changes. BiTlSe is a trivial insulator when $\delta < 0.47$. All of the parities at the corners are positive, and each Bloch state can have two spins. There is a band inversion when $\delta = 0.47$, causing the parity at the origin to change sign. As a result, the material becomes a topological insulator. It now has helical edge states, in which the direction of spin is locked with the direction of momentum (see the ARPES data in dark insets). Fig from Xu *et al.*, 2011

A. Fermi circle of the surface state

To understand the implication of these δ_i-parities on the eight corners, we can rely on the knowledge acquired in the past two chapters. First, for a 1D spin pump, we know that if $\Delta P_\theta = P_\theta(T/2) - P_\theta(0) = 1$ mod 2, then an edge state would traverse the energy gap (Fig. 3(a)). Similar traversing of an edge state across the energy gap occurs in a 2D topological insulator (Fig. 3(b)).

We now consider 3D topological insulator. In Fig. 3(c), four examples of the cumulative parity distributions at TRIM are shown. The product of all 8 parities gives $(-1)^{\nu_0}$. The product of four cumulative parities on the k_y-k_z plane at $k_x = \pi$ gives $(-1)^{\nu_1}$, and so on. This way, one can get the four indices $(\nu_0; \nu_1, \nu_2, \nu_3)$ shown on top of the figures.

Next, cut the TI open with a surface perpendicular to the z-axis. Fig. 3(d) shows the 2D surface BZ of the surface state (SS) on the k_x-k_y plane.The parities π_i on corners are the products of two parities along the k_z-direction. Write $\pi_1 = (-1)^{P_{\theta 1}}$, where $P_{\theta 1}$ is the TR polarization at $(k_x, k_y) = 0$ of a 1D sub-system along the z-direction; similarly $\pi_2 = (-1)^{P_{\theta 2}}$. The k_x or k_y plays the role of the time in the Fu-Kane spin pump (Fig. 3(a)). Therefore, when $\Delta P_\theta = P_{\theta 2} - P_{\theta 1} = 1$ mod 2, or $\pi_1 \pi_2 = -1$ (e.g., see the 2nd figure from the left in Fig. 3(d)). There is one (or an odd number of) edge state traversing the energy gap from $k_x = 0$ to π, crossing the chemical potential μ at a Fermi point, similar to Fig. 3(b)). On the other hand, since $\pi_1 \pi_3 = 1$, there is no (or an even number of) edge state crossing μ. The Fermi point at $k_y = 0$ becomes a Fermi line when one scans over k_y.

Therefore, once we know the four parities π_i, the topology of the Fermi circle in the 2D surface BZ can be determined (assuming the energy dispersion of a SS crosses the Fermi level only once): between a black dot (odd parity) and a white dot (even parity), there must be a Fermi line separating filled states from empty states. One can check that the Fermi circles in Fig. 3(d) do follow this rule. The Fermi sea encloses one or more black dots, which are also the locations of Dirac points (in 2D momentum space).

Fig. 4 sums up nicely what we have learned so far. When the compound BiTlSe undergoes a phase transition from an ordinary insulator to a strong TI, the band inversion, the change of parity at TRIM, and the helical surface states with spin-momentum locking all emerge simultaneously.

In general, a strong TI would have odd number of Dirac points, and odd pairs of helical SS. On the other hand, a weak TI always have even number of Dirac points, and even pairs of helical SS. The Dirac point of a weak TI is fragile. Take the one with indices $(0; 011)$ as an example: Suppose that due to *surface reconstruction*, a unit cell is doubled along the y-direction. As a result, the surface BZ would be folded back along the k_y-direction. The two black dots now could couple with each other and open the Dirac point.

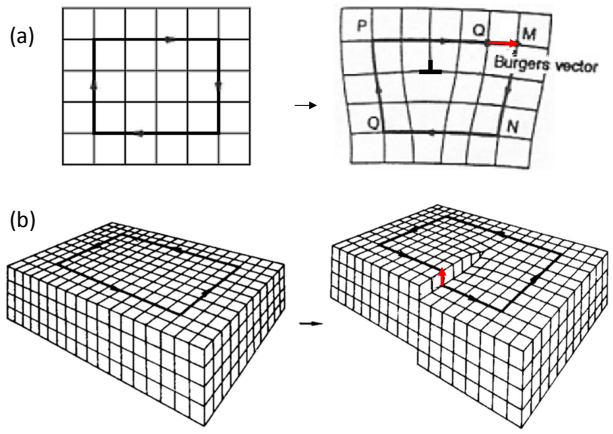

FIG. 5 (a) For a lattice with an edge dislocation, the Burgers vector is perpendicular to the line of dislocation. (b) For a lattice with screw dislocation, the Burgers vector is parallel to the line of dislocation.

Note that even though for a strong TI, there are odd number of Dirac points on *one* surface, there are more Dirac points on the opposite side of the TI. When counted together, a 3D TI would still have even number of Dirac points from its surface states.

BiSb is the first experimentally confirmed 3D topological insulator (Hsieh *et al.*, 2008). Subsequently, many more have been predicted and verified (Bansil *et al.*, 2016). An ideal TI would be one that is an *insulator* with *large band gap*. But this is hard to come by, because the inversion of energy gap is often a result of spin-orbit coupling, which is not easy to be enhanced. More comments on topological materials can be found in Sec. I.D below.

B. Weak topological indices

As we have mentioned earlier, a weak TI with indices $(0;0,0,1)$ can be considered as layers of 2D TIs stacked along the z-axis. For general weak indices, one can define

$$\mathbf{M}_\nu = \nu_1 \frac{\mathbf{g}_1}{2} + \nu_2 \frac{\mathbf{g}_2}{2} + \nu_3 \frac{\mathbf{g}_3}{2}, \tag{1.8}$$

in which $\mathbf{g}_i$ are basis of reciprocal lattice vectors, then the 2D-TI layers are stacked along the $\mathbf{M}_\nu$ direction.

Even though a weak 3D TI has fragile 2D surface states, it can have robust 1D states along a line of dislocation. In Fig. 5, one can see that due to a line of dislocation along $\mathbf{t}$, a loop that is closed in a perfect crystal now can no longer be closed. The vector of displacement $\mathbf{B}$ is called a **Burgers vector**. For an **edge dislocation**, $\mathbf{B} \perp \mathbf{t}$; for a **screw dislocation**, $\mathbf{B} \parallel \mathbf{t}$.

It is shown by Ran *et al.*, 2009 that, if

$$\mathbf{B} \cdot \mathbf{M}_\nu = \pi \pmod{2\pi}, \tag{1.9}$$

then there is a pair of helical edge states along the line of dislocation (Fig. 6). For example, consider a cubic lattice

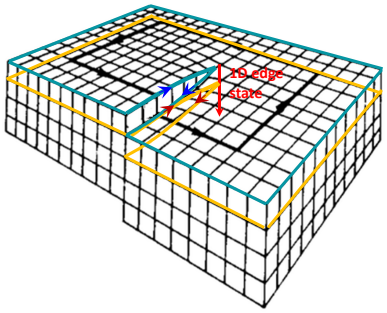

FIG. 6 In a 3D weak TI with screw dislocation, each plane can be considered as a 2D insulator with a cut ending at the line of dislocation. Near the cut, the opposing edge channels from adjacent planes cancel with each other. As a result, the edge electrons would move down the line of dislocation.

with indices $(0;0,0,1)$, then $\mathbf{M}_\nu = \mathbf{g}_3/2 = \pi/a\hat{z}$, where a is the lattice constant. If there is a screw dislocation with $\mathbf{B} = a\hat{z}$ (see Fig. 5(b)), then $\mathbf{B} \cdot \mathbf{M}_\nu = \pi$, and there are 1D helical states along the line of dislocation. If $\mathbf{B} = a\hat{x}$ or $a\hat{y}$ (for edge dislocation), then there is no edge state in this weak TI.

This criterion applies to both strong and weak TIs. For example, if $\nu_0 = 1$, but $\mathbf{M}_\nu = 0$, then none of the dislocation lines would have helical edge states.

C. Bulk-edge correspondence

Surface (or edge) state has been a recurring theme in this course. At the interface between two materials with different quantum topological phases, the interface states are bound to exist. This is called the **bulk-edge correspondence**. So far, we have discussed the domain-wall state in SSH model, the chiral edge state in quantum Hall system, the edge state in Fu-Kane spin chain, and the helical edge states in 2D and 3D TIs. We will see more examples of surface state later, when new topological phases are encountered.

Even though a general proof is lacking, such a bulk-edge correspondence is generally believed to be true (for *non-interacting* systems). This property can roughly be understood as follows: In the sense of Thomas-Fermi approximation, energy gap can be defined locally and vary with location. Near the interface between two different topological phases, the energy gap needs to close (e.g., for band inversion), otherwise the topological phase could not change. As a result, there must be a gapless region near the interface (or surface) for electrons to dwell on.

A remark: For a quantum topological phase to change, the energy gap needs be closed. Such a statement is valid only if the symmetry of the system remains unchanged. *If* the symmetry changes, then can pass from one phase to the other *without* closing the gap (Ezawa *et al.*, 2013). For example, consider the SSH model,

$$H = (t_- + t_+ \cos k)\sigma_x + t_+ \sin k\ \sigma_y + m\sigma_z, \tag{1.10}$$

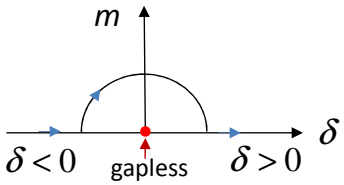

FIG. 7 In the parameter space of (δ, m), the SSH model is gapless only at a single point $(0, 0)$.

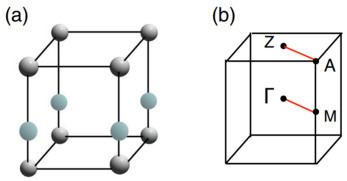

FIG. 8 (a) Tetragonal lattice with two different atoms in the unit cell. (b) Four high symmetry points in a BZ. Fig. from Fu, 2011.

where $t_\pm = t \pm \delta$, δ is the dimerization parameter (see Prob. 2 of Chap **??**). The energy spectrum is

$$E_\pm = \pm\sqrt{t^2 \cos^2 \frac{k}{2} + \delta^2 \sin^2 \frac{k}{2} + m^2}. \tag{1.11}$$

When $m = 0$, H has both TRS and particle-hole symmetry. To get from the phase with $\delta > 0$ to the one with $\delta < 0$, we need to cross the gapless point $(\delta, m) = (0, 0)$, see Fig. 7. However, if $m \neq 0$, then H has no TRS and the energy bands are gapped. In this case, one can go from a phase with $\delta > 0$ $(m = 0)$ to a phase with $\delta < 0$ $(m = 0)$ via a path with non-zero m, such that the energy gap remains open during the transit.

D. Topological crystalline insulator and beyond

In addition to TRS, the topology of an insulator can also be protected by crystalline symmetry. These are called **topological crystalline insulator** (TCI). As we have learned, $T^2 = -1$ plays a crucial role in TI. In a TCI, this is not required and $T^2 = 1$ is allowed. That is, electron spin, as well as spin-orbit coupling, is no longer essential to the topology.

The crystalline symmetry can be mirror symmetry, rotation symmetry (from 3-fold rotation, 4-fold rotation etc), or more general types of spatial symmetry. Fu, 2011 studied a tetragonal crystal with 4-fold rotation symmetry (Fig. 8(a)). His theory is briefly sketched below.

The operator for C_4 rotation is $U = e^{i\frac{\pi}{2}L_z}$, which has eigenvalues $+1, -1, +i$, and $-i$. The TR operator is $T = K$ for spinless electron, and $T^2 = 1$. There are 4 special momenta $\mathbf{k}_i$'s in the 3D BZ that are invariant under U and T (Fig. 8(b)), which play a role similar to the TRIM.

First, since $[H(\mathbf{k}_i), U] = 0$ at the 4 $\mathbf{k}_i$'s, energy eigenstates can be labelled by the eigenvalues of U. Second, $\mathbf{k}_i$'s are invariant under TR,

$$TH(\mathbf{k}_i)T^{-1} = H(-\mathbf{k}_i) = H(\mathbf{k}_i). \tag{1.12}$$

Together with $T^{-1} = T$, this implies that $H(\mathbf{k}_i)$ must be real-valued. Thus one can always choose its eigenvalues to be real. That is, complex eigenvalues $+i, -i$ of U must appear in pair. This pair of states form a *2D irreducible real representation*, which is similar to a Kramer pair. For this pair, we have $U^2 = -1$ and $(UT)^2 = -1$.

Define the sewing matrix,

$$v_{mn}(\mathbf{k}_i) = \langle u_m(\mathbf{k}_i)|UT|u_n(\mathbf{k}_i)\rangle, \tag{1.13}$$

where $\mathbf{k}_i$ is one of the special momenta. The topological invariant ν_0 is given by,

$$(-1)^{\nu_0} = (-1)^{\Gamma M}(-1)^{AZ}, \tag{1.14}$$

where

$$(-1)^{\nu_{\mathbf{k}_1\mathbf{k}_2}} = \exp\left(i\int_{\mathbf{k}_1}^{\mathbf{k}_2} d\mathbf{k}\cdot \mathrm{tr}\ \mathsf{A}(\mathbf{k})\right)\frac{\mathrm{pf}[\mathsf{v}(\mathbf{k}_2)]}{\mathrm{pf}[\mathsf{v}(\mathbf{k}_1)]}, \tag{1.15}$$

where $\mathsf{A}(\mathbf{k})$ is the non-Abelian Berry connection. The Z_2 integer ν_0 is invariant under gauge transformation. When $\nu_0 = 1$, we have a TCI with robust surface state on the surface that respects the rotation symmetry.

The surface states need to cross each other at $\mathbf{k}_i$, similar to the SS in a topological insulator. However, some other aspects of the SS are different. For example, their energy dispersion near the crossing point is quadratic in Fu's example, instead of linear. Also, the number of Dirac points on a surface can be even, instead of odd. Note that even though the gapless Dirac point is protected by the UT symmetry, the rotation symmetry could be damaged by structural deformation.

In some other TCIs, the TR symmetry can be dispensed with, so that only the crystalline symmetry is at play. The first experimentally confirmed TCI is SnTe (Hsieh *et al.*, 2012), which is protected by a mirror symmetry.

This discovery opens up a floodgate to topological materials, since there are hundreds of crystalline symmetry groups. With the help of the so-called *symmetry-based indicators* (Po *et al.*, 2017) or *elementary band representations* (Bradlyn *et al.*, 2017), researchers can search through the database of materials to find out candidates of topological materials. See Gibney, 2018, Tang *et al.*, 2019, and Queiroz and Stern, 2020 for some updates.

A related development is the discovery of **higher-order TCIs**. They have conducting SS protected by topology along edges (2nd order), or corners (3rd order) of the topological material. Also, see Parameswaran and Wan, 2017 and the references therein.

The topology in TI and TCI are protected by time-reversal symmetry and crystalline symmetry. They belong to a larger class of topological phases called **symmetry-protected topological (SPT) phases**. The famous **Haldane phase** of odd-integer spin chain is another example of the SPT phase. It is protected by

SO(3) spin symmetry. In addition, there are also topological phases *not* related to (and protected by) symmetry, such as the **fractional quantum Hall state**.

References

Bansil, A., H. Lin, and T. Das, 2016, Rev. Mod. Phys. **88**, 021004.

Bradlyn, B., L. Elcoro, J. Cano, M. G. Vergniory, Z. Wang, C. Felser, M. I. Aroyo, and B. A. Bernevig, 2017, Nature **547**, 298 EP .

Ezawa, M., Y. Tanaka, and N. Nagaosa, 2013, Scientific Reports **3**, 2790 EP .

Fu, L., 2011, Phys. Rev. Lett. **106**, 106802.

Fu, L., and C. L. Kane, 2007, Phys. Rev. B **76**, 045302.

Fu, L., C. L. Kane, and E. J. Mele, 2007, Phys. Rev. Lett. **98**, 106803.

Gibney, E., 2018, Nature **560**, 151.

Hsieh, D., D. Qian, L. Wray, Y. Xia, Y. S. Hor, R. J. Cava, and M. Z. Hasan, 2008, Nature **452**(7190), 970.

Hsieh, T. H., H. Lin, J. Liu, W. Duan, A. Bansil, and L. Fu, 2012, Nature Communications **3**, 982.

Moore, J. E., and L. Balents, 2007, Phys. Rev. B **75**, 121306.

Parameswaran, S., and Y. Wan, 2017, Physics **10**, 1.

Po, H. C., A. Vishwanath, and H. Watanabe, 2017, Nature Communications **8**(1), 50.

Queiroz, R., and A. Stern, 2020, Symmetry indicators for topological superconductors, journal Club for Condensed Matter Physics: www.condmatjclub.org/?p=4161.

Ran, Y., Y. Zhang, and A. Vishwanath, 2009, Nat. Phys. **5**, 298.

Roy, R., 2009, Phys. Rev. B **79**, 195322.

Tang, F., H. C. Po, A. Vishwanath, and X. Wan, 2019, Nature Physics **15**(5), 470.

Xu, S.-Y., Y. Xia, L. A. Wray, S. Jia, F. Meier, J. H. Dil, J. Osterwalder, B. Slomski, A. Bansil, H. Lin, R. J. Cava, and M. Z. Hasan, 2011, Science **332**(6029), 560.